
This is an electronic reprint of the original article.
This reprint may differ from the original in pagination and typographic detail.

Khayyami, Aida; Karppinen, Maarit

Reversible Photoswitching Function in Atomic/Molecular-Layer-Deposited ZnO:Azobenzene Superlattice Thin Films

Published in:
Chemistry of Materials

DOI:
[10.1021/acs.chemmater.8b01833](https://doi.org/10.1021/acs.chemmater.8b01833)

Published: 17/08/2018

Document Version
Publisher's PDF, also known as Version of record

Published under the following license:
CC BY

Please cite the original version:
Khayyami, A., & Karppinen, M. (2018). Reversible Photoswitching Function in Atomic/Molecular-Layer-Deposited ZnO:Azobenzene Superlattice Thin Films. *Chemistry of Materials*, 30(17), 5904–5911. Article 1. <https://doi.org/10.1021/acs.chemmater.8b01833>

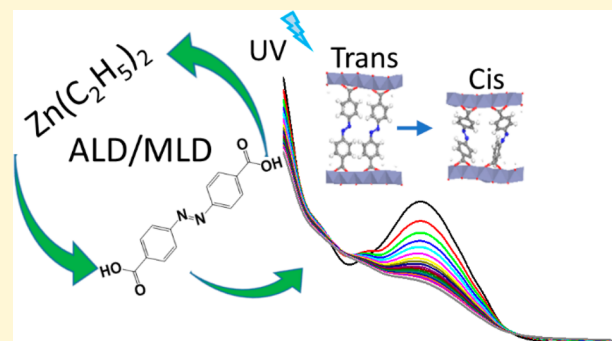
This material is protected by copyright and other intellectual property rights, and duplication or sale of all or part of any of the repository collections is not permitted, except that material may be duplicated by you for your research use or educational purposes in electronic or print form. You must obtain permission for any other use. Electronic or print copies may not be offered, whether for sale or otherwise to anyone who is not an authorised user.

Reversible Photoswitching Function in Atomic/Molecular-Layer-Deposited ZnO:Azobenzene Superlattice Thin Films

Aida Khayyami and Maarit Karppinen*¹

Department of Chemistry and Materials Science, Aalto University, P.O. Box 16100, FI-00076 Aalto, Finland

ABSTRACT: We report new types of reversibly photoresponsive ZnO:azobenzene superlattice thin films fabricated through atomic/molecular-layer deposition (ALD/MLD) from diethylzinc, water, and 4,4'-azobenzene dicarboxylic acid precursors. In these ultrathin films, crystalline ZnO layers are interspersed with monomolecular photoactive azobenzene dicarboxylate layers. The thickness of the individual ZnO layers is precisely controlled by the number (m) of ALD cycles applied between two subsequent MLD cycles for the azobenzene layers; in our $\{[(\text{Zn}-\text{O})_m+(\text{Zn}-\text{O}_2-\text{C}-\text{C}_6\text{H}_4-\text{N}=\text{N}-\text{C}_6\text{H}_4-\text{C}-\text{O}_2)]_n+(\text{Zn}-\text{O})_m\}$ samples, m ranges from 0 to 240. The photoresponsive behavior of the films is demonstrated with ultraviolet–visible spectroscopy; all the films are found to be photoreactive upon 360 nm irradiation, the kinetics of the resultant trans–cis photoisomerization somewhat depending on the superlattice structure. The reversibility of the photoisomerization reaction is then confirmed with a subsequent thermal treatment. Our work thus provides proof-of-concept evidence of the suitability of the ALD/MLD technology for the implementation of photoactive moieties such as azobenzene within an inorganic matrix as an attractive new methodology for creating novel light-switchable functional materials.



1. INTRODUCTION

Certain polymers and organic molecules have the capability to respond to tiny changes in their environment (e.g., temperature, light exposure, electric or magnetic field, humidity, or pH) with a measurable change in some intrinsic property, such as color, shape, electrical conductivity, or water permeability. This stimulus-responsive behavior is a highly attractive phenomenon for a number of potential applications; in particular, light-stimulated or so-called photoresponsive materials have been investigated for new types of optical switches,^{1,2} data storage devices,^{3,4} nanovalves,⁵ sensors,⁶ and local drug dispensers.^{7–9} Thus, the direct noncontact manipulation of photoresponsive materials through light illumination is an attractive phenomenon in itself. In addition, we may imagine hybrid materials in which the photoresponsive organic component is embedded in an inorganic matrix in such an intimate way that the photostimulated change in, e.g., the size of the photoresponsive organics would switch on an action in the inorganic host material. Such control-embedded hybrid materials could open up exciting new horizons in designing novel functional nanodevices.^{10–12}

The azobenzene moiety $\text{C}_6\text{H}_5-\text{N}=\text{N}-\text{C}_6\text{H}_5$, consisting of a diazene– $\text{N}=\text{N}$ –bridge between two phenyl groups, is one of the prototype photoresponsive components. It isomerizes reversibly around the $\text{N}=\text{N}$ bond upon irradiation with light of different wavelengths.^{13,14} This trans–cis photoisomerization from the more stable trans form to the less stable cis form is accompanied by a remarkable structural change, which has inspired several research groups to challenge azobenzene and

its derivatives as photoswitchers for various smart materials.¹⁵ The two isomers exhibit distinct absorption bands in the ultraviolet–visible (UV–vis) region and also several other differences in physical properties, including their different dielectric constants and dipole moments.¹⁶

Efforts to incorporate azobenzene molecules into inorganic matrices, such as layered double hydroxides,^{12,17–19} HfS_2 ,²⁰ Fe_3O_4 ,²¹ GeO_2 ,² TiO_2 ,^{10,22} and ZnO ,²³ have indeed been made, and in particular in the case of the two-dimensional matrices with an anticipation that the weakly polar interlayer galleries would provide the azobenzene molecules with an optimal alignment and sufficient free space for the shape change to occur.^{12,18} For the incorporation of azobenzene moieties in inorganic hosts, various conventional solution-based techniques, such as Langmuir–Blodgett,²⁴ sol–gel,^{10,21} and layer-by-layer electrostatic self-assembly,¹⁸ have been used. However, the apparent needs to enhance the intimate interaction between the organic switcher molecules and the inorganic matrix and to manipulate, preferably with atomic/molecular level accuracy, the organic-to-inorganic ratio and distribution call for fundamentally novel synthesis approaches.²⁵ In particular, high-end gas-phase thin film techniques could allow not only the precise chemical control of the inorganic–azobenzene interfaces but also the integration

Received: May 3, 2018

Revised: August 15, 2018

Published: August 17, 2018

of these materials into microelectronics and other advanced technologies.

Here we demonstrate for the first time that the state-of-the-art gas-phase atomic/molecular-layer deposition (ALD/MLD) technique²⁶ is superbly suited for the fabrication of precisely layer-engineered thin films in which monomolecular azobenzene layers are coherently connected via covalent chemical bonds to the surfaces of accurately thickness-tuned metal oxide layers. This technique is derived from the conventional ALD (atomic-layer deposition) thin film technology,^{27,28} already used for decades for industrial-scale production of high-quality thin films and coatings of simple inorganic materials. In ALD, two (or more) mutually reactive gaseous/evaporated precursors are pulsed into the reactor chamber one after another with intermediate purging, which results in self-limited gas-surface reactions and enables the fabrication of high-quality thin films of well-defined composition and thickness even on large-area substrates. The resultant thin film coatings are moreover highly conformal, following nearly perfectly various surface architectures down to their nanometer precision.^{28,29} A similar technique, i.e., MLD (molecular-layer deposition), for purely organic thin films has also been known, though much less exploited, since 1990s.^{30,31} Then, in the more recently developed ALD/MLD technique for hybrid thin films, ALD and MLD cycles are combined to produce alternate inorganic and organic layers with atomic/molecular level precision.^{32,33} Most interestingly, the combined ALD/MLD technique allows the engineering of carefully designed inorganic–organic multilayer structures as its self-limiting gas-surface reactions enable the precise control of the introduction frequency of the organic layers within the inorganic matrix.^{34–36} This has already been demonstrated with various superlattice, nanolaminate, and gradient structures, investigated for, e.g., gas-barrier^{37–39} and thermal-barrier^{40–42} coatings, as well as for tuning the optical properties.^{43,44} Moreover, from the multiple positive experiences related to the conventional ALD technique for inorganics, we may anticipate that the ALD/MLD processes for novel inorganic–organic thin films should also be feasible for industry.

We chose the ZnO:azobenzene system as our model system because (i) ZnO has unique (photo)physical properties such as a direct band gap of 3.37 eV along with tunable optical and electronic properties,^{45–47} (ii) ZnO is one of the prototype ALD thin film materials^{45,48,49} and also well-behaving Zn-based ALD/MLD processes have already been developed,^{50–54} and (iii) azobenzene moieties have been successfully combined with ZnO using conventional synthesis techniques.^{23,45,55–57} However, while the hybrid film growth principle is exactly the same as with the other already known ALD/MLD processes, the challenge here is the considerably larger size of the azobenzene moiety compared to the typical organic components so far employed in ALD/MLD. The higher sublimation temperature thus required for the organic precursor restricts the depositions to the higher temperatures and may thus introduce additional concerns for the choice of the inorganic precursor and the substrate materials. We therefore first carefully optimize our ALD/MLD for the selected Zn and azobenzene precursors. We investigate ZnO:azobenzene superlattice (SL) structures within a wide composition range. X-ray reflectivity and infrared spectroscopy are employed to verify the intended superlattice structures, and the reversible photoisomerization of the films is demonstrated through UV–vis spectroscopy observations.

2. EXPERIMENTAL SECTION

2.1. Thin Film Depositions. All the thin film depositions were performed in a commercial flow type hot-wall ALD reactor (F-120 by ASM Microchemistry Ltd.) using diethylzinc $\text{Zn}(\text{C}_2\text{H}_5)_2$ (DEZ; Aldrich, 52 wt % Zn at minimum), water, and azobenzene-4,4'-dicarboxylic acid (AzB-DCA; TCI, 95%) as precursors. To reach the precursor vapor pressures required for the efficient transport of the precursor to the substrate, AzB-DCA was placed in an open boat inside the reactor and heated to 310 °C for sublimation, whereas DEZ and H_2O were evaporated using external reservoirs held at room temperature. Nitrogen (>99.999%, Schmidlin UHPN 3000 N_2 generator) was used as a carrier and purging gas. The depositions were performed under a 3–4 mbar pressure onto Si(100) and quartz slide substrates; the latter substrates were used for the UV–vis transmittance spectroscopy measurements.

The ALD cycle for the ZnO layers was DEZ for 1 s, N_2 for 1.5 s, H_2O for 1.5 s, and N_2 for 2 s,⁵⁸ and the ALD/MLD cycle for the $(\text{Zn}-\text{O}_2-\text{C}-\text{C}_6\text{H}_4-\text{N}=\text{N}-\text{C}_6\text{H}_4-\text{C}-\text{O}_2)$ layers was DEZ for 3 s, N_2 for 4 s, AzB-DCA for 10 s, and N_2 for 40 s, unless otherwise stated for the different precursor pulse lengths investigated. Then, to fabricate the superlattice films, the aforementioned ALD cycles for ZnO layers were combined with the ALD/MLD cycles for the Zn:azobenzene layers as follows: $\{[(\text{DEZ}+\text{H}_2\text{O})_m+(\text{DEZ}+\text{sAzB-DCA})_n+(\text{DEZ}+\text{H}_2\text{O})_m]\}_n$. This is expected to yield $\{[(\text{Zn}-\text{O})_m+(\text{Zn}-\text{O}_2-\text{C}-\text{C}_6\text{H}_4-\text{N}=\text{N}-\text{C}_6\text{H}_4-\text{C}-\text{O}_2)_n+(\text{Zn}-\text{O})_m]\}_n$ SL structures in which single molecular azobenzene layers are sandwiched between wider ZnO-layer blocks with a controlled thickness (m cycles); note that n is the number of repetitions of the superlattice cycle and thus indicates the total number of monomolecular azobenzene layers in the film. Superlattice thin films with m ranging from 0 to 240 and n ranging from 4 to 150 were deposited through different combinations of the individual DEZ+ H_2O ALD and DEZ+AzB-DCA ALD/MLD cycles.

2.2. Characterization Techniques. The film thicknesses, roughnesses, and densities were determined through X-ray reflectivity (XRR; X'Pert MPD PRO Alfa 1, PANalytical) measurements. The XRR data were fitted by X'Pert Reflectivity software by PANalytical for the film thickness and roughness; the thickness value was further divided by the number of deposition cycles to obtain the film growth rate, or the so-called growth-per-cycle (GPC) value. The density of the films was calculated from the XRR patterns based on the dependency of critical angle θ_c on mean electron density ρ_e of the film material, namely, $\rho_e = (\theta_c^2 \pi) / (\lambda^2 r_e)$, where λ is the X-ray wavelength and r_e is the classical electron radius. The degree of crystallinity of the films was investigated by grazing incidence X-ray diffraction (GIXRD; X'Pert MPD PRO Alfa 1, PANalytical; Cu $K\alpha$ radiation) with the incident angle ranging from 20° to 70°. The chemical composition of the films was analyzed using Fourier transform infrared (FTIR; Nicolet Magna 750) spectroscopy; the measurement chamber was continuously purged with purified dry air during the measurements. A background spectrum was collected using an uncoated Si wafer and subtracted from the spectra measured for the samples.

Photoisomerization of the films was investigated under irradiation by UV light using a 200 W xenon-doped mercury lamp (Hamamatsu Lightning cure LC8) equipped with a cutoff filter ($\lambda = 300\text{--}480$ nm). The photon flux was 3000 mW/cm^2 (at a working distance of 10 mm). For these measurements, the samples were grown on quartz substrates. The UV–vis transmittance spectra (Shimadzu UV-2600 spectrometer) were recorded for samples in the wavelength range of 200–600 nm. To investigate the cis-to-trans back-isomerization reaction, the samples were heated in air at 100 °C for 24 h.

3. RESULTS AND DISCUSSION

We deposited a series of $\{[(\text{Zn}-\text{O})_m+(\text{Zn}-\text{O}_2-\text{C}-\text{C}_6\text{H}_4-\text{N}=\text{N}-\text{C}_6\text{H}_4-\text{C}-\text{O}_2)_n+(\text{Zn}-\text{O})_m]\}_n$ thin films from diethylzinc, water, and azobenzene dicarboxylic acid precursors (see Table 1 and Figure 1); the depositions yielded visually homogeneous thin films for all values of m and n that were

Table 1. $\{[(\text{Zn}-\text{O})_m+(\text{Zn}-\text{O}_2-\text{C}-\text{C}_6\text{H}_4-\text{N}=\text{N}-\text{C}_6\text{H}_4-\text{C}-\text{O}_2)_n+(\text{Zn}-\text{O})_m]\}$ Film Structures Deposited in This Work at 320 °C

film type	n	m	expected ZnO-layer thickness (nm)	$n(m+1)+m$	total film thickness (nm)	GPC (Å/cycle)
ZnO	0	1000	130	1000	130	1.30
SL	4	240	31	1200	143	1.20
SL	6	171	22	1197	137	1.15
SL	10	90	12	990	122	1.25
SL	15	37	5	592	92	1.55
SL	30	19	2.5	589	103	1.75
SL	60	10	1.3	610	120	1.95
SL	150	4	0.52	604	164	2.70
hybrid	200	0	0	200	60	3.00
hybrid	300	0	0	300	92	3.00
hybrid	400	0	0	400	125	3.10
hybrid	600	0	0	600	192	3.20

investigated. In the following, we first discuss the optimization of the ALD/MLD process parameters of the DEZ+AzB-DCA process for the hybrid $(\text{Zn}-\text{O}_2-\text{C}-\text{C}_6\text{H}_4-\text{N}=\text{N}-\text{C}_6\text{H}_4-\text{C}-\text{O}_2)_n$ films with $m = 0$, investigate the possibility of combining this process with the well-known DEZ+H₂O ALD process for different SL structures with $m > 0$, and finally characterize the basic chemical and structural properties and the photoresponse behaviors of the resultant thin films.

3.1. ALD/MLD Process Parameters. We first confirmed the fulfillment of the surface saturation criterion for both precursors in our DEZ+AzB-DCA process by gradually increasing the pulse length of one of the precursors at a time while keeping the pulse length for the other precursor fixed and then monitoring the possible changes in the GPC value accordingly (see Figure 2a). These experiments were performed at 320 °C, which is the lowest feasible deposition temperature for the DEZ+AzB-DCA process, defined by the relatively high evaporation temperature of AzB-DCA (310 °C).

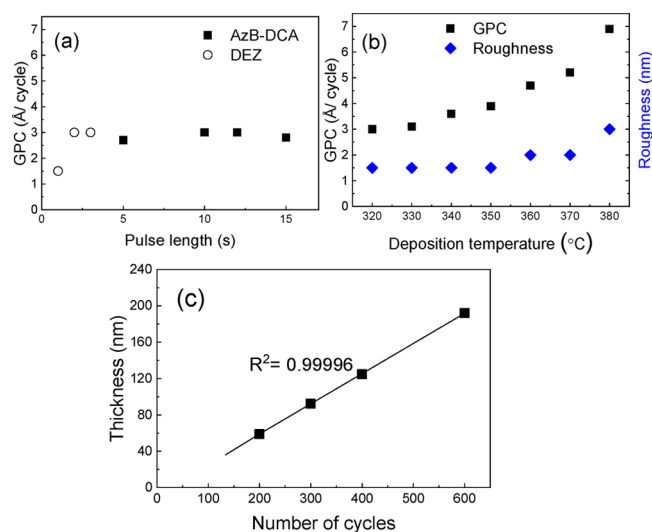


Figure 2. Optimization of ALD/MLD parameters: (a) GPC as a function of the precursor pulse lengths of DEZ (AzB-DCA for 10 s) and AzB-DCA (DEZ for 3 s) at 320 °C, (b) GPC and surface roughness values at different deposition temperatures (pulse sequence of DEZ for 3 s, N₂ for 4 s, AzB-DCA for 10 s, and N₂ for 40 s), and (c) film thickness vs the number of ALD/MLD cycles at 320 °C. In panels a and b, the number of ALD/MLD cycles was 300.

On the basis of Figure 2a, the surface reactions reach saturation in 2 s for DEZ and in 10 s for AzB-DCA. For the rest of the experiments, we fixed the pulse/purge lengths as follows: DEZ for 3 s, N₂ for 4 s, AzB-DCA for 10 s, and N₂ for 40 s.

Next we investigated the growth rate at different deposition temperatures (see Figure 2b). It was found that the GPC value of ~ 3 Å/cycle at 320 °C gradually increases with an increasing deposition temperature, up to ~ 7 Å/cycle at 380 °C, possibly because of some CVD type growth. Also revealed in Figure 2b is the fact that the surface roughness increases with an increasing deposition temperature; at ≥ 390 °C, the films were

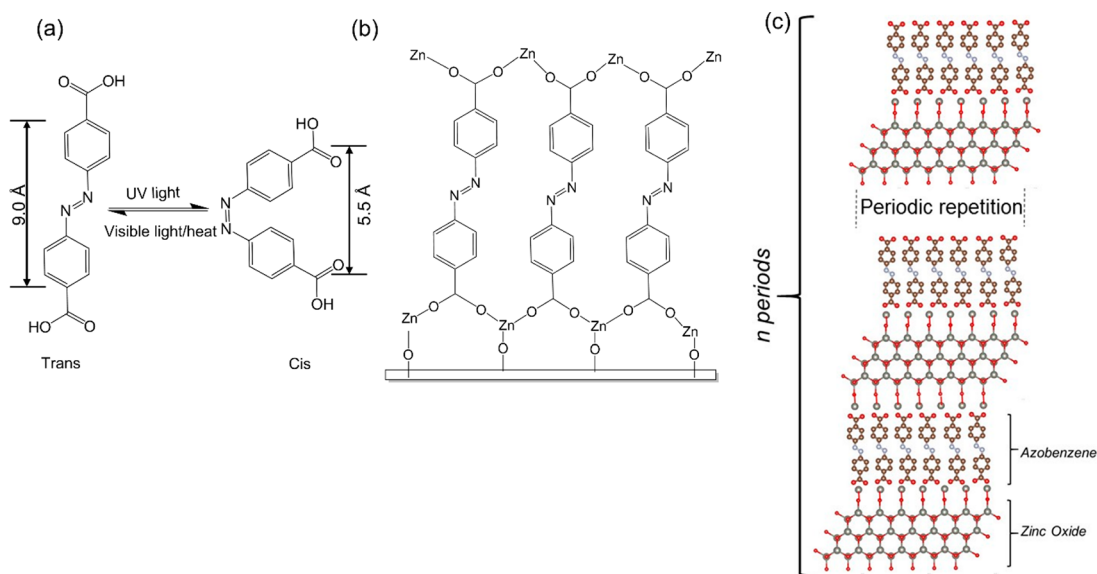


Figure 1. (a) Structure of the trans and cis isomers of the AzB-DCA precursor and schematic two-dimensional illustrations of (b) the bonding structure in the hybrid $m = 0$ film and (c) the $\{[(\text{Zn}-\text{O})_m+(\text{Zn}-\text{O}_2-\text{C}-\text{C}_6\text{H}_4-\text{N}=\text{N}-\text{C}_6\text{H}_4-\text{C}-\text{O}_2)_n+(\text{Zn}-\text{O})_m]\}$ superlattice structure with $m = 3$.

so rough that they could no longer be reliably studied by XRR. For the rest of the experiments, we fixed the deposition temperature to 320 °C. To confirm the ideal ALD/MLD type growth at this temperature, we finally deposited a series of hybrid films by applying different numbers of DEZ+AzB-DCA cycles. Figure 2c shows that the film thickness increases linearly with an increasing number of cycles, which indicates an excellent atomic/molecular level control over the film thickness.

3.2. Characterization of $m = 0$ Hybrid Films. From GIXRD measurements, all the hybrid $m = 0$ films deposited via the DEZ+AzB-DCA process in the temperature range of 320–380 °C were found to be amorphous. The film density of the hybrid film deposited at 320 °C was determined from the XRR data to be ~ 1.5 g/cm³, which is less than one-third of the ideal density of bulk wurtzite-structured ZnO (5.6 g/cm³) and the density determined for our crystalline ZnO film deposited at 320 °C (5.0 g/cm³); this is what one could expect as the films are composed of zinc ions in combination with light and spacious organic molecules instead of single negatively charged oxide ions. All the films independent of the deposition temperature were homogeneous in appearance and stable under ambient conditions. A representative film deposited at 320 °C was reanalyzed after storage for one month and found to be unaltered.

In panels a and b of Figure 3, we display FTIR and UV–vis spectra for our hybrid $m = 0$ film deposited at 320 °C to confirm the presence of the azobenzene moieties in the film.

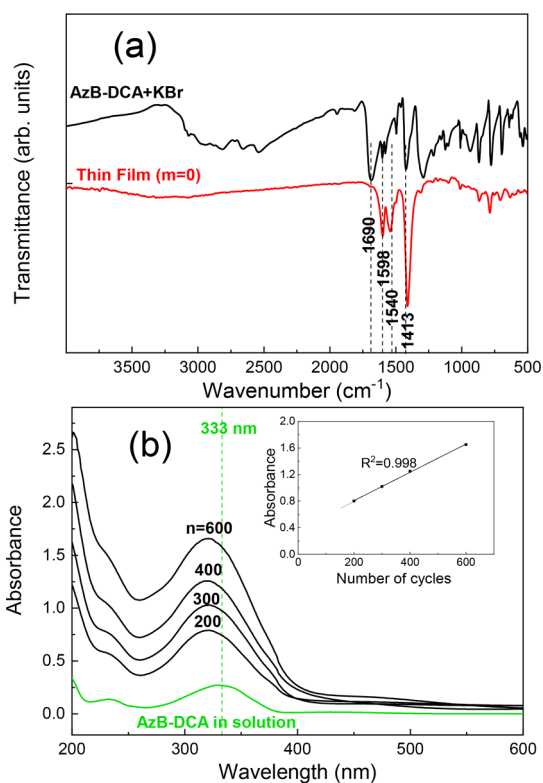


Figure 3. (a) FTIR spectra for a representative (92 nm) hybrid $m = 0$ film (deposited on silicon) and also for the AzB-DCA precursor powder (mixed with KBr) for reference. (b) UV–vis absorption spectra of hybrid films with varying numbers of ALD/MLD cycles. The green line shows the spectrum of AzB-DCA in aqueous solution. In the inset, the absorbance of the films at λ_{\max} is plotted vs the number of cycles.

Also given are the spectra recorded for the 4,4'-azobenzene dicarboxylic acid precursor for comparison. The disappearance of the sharp signal at 1690 cm⁻¹ in the FTIR spectrum of the thin film sample that is characteristic of the C=O stretching of free carboxylic acids confirms the bonding of the organic precursor to the zinc cation through this unit upon formation of the hybrid thin film. At the same time, the fact that the absorption band seen at 3200–3500 cm⁻¹ in the spectrum of the precursor due to the OH group is missing from the spectrum of the hybrid thin film indicates that the azobenzene moiety is bonded to Zn through the oxygen atom from the carboxylate OH group as well to form the (Zn–O₂–C–C₆H₄–N=N–C₆H₄–C–O₂)_n hybrid film, as shown in Figure 1b. Finally, we note that the splitting between the dominant absorption peaks at 1413 and 1598 cm⁻¹ due to the symmetric and asymmetric stretchings of the carboxylate group, respectively, is 185 cm⁻¹, which confirms that the carboxylate group is indeed in a bridging position between two zinc cations.^{59,60}

The UV–vis absorption spectra for the AzB-DCA precursor (in aqueous solution) and our hybrid $m = 0$ films with various thicknesses corresponding to ALD/MLD cycle numbers (n) of 200, 300, 400, and 600 are depicted in Figure 3b. The strong absorption band seen at ~ 320 nm for the AzB-DCA precursor is due to the π – π^* transition in the azobenzene trans isomer.^{18,24} For our hybrid (Zn–O₂–C–C₆H₄–N=N–C₆H₄–C–O₂)_n thin films, this transition shows a 10 nm blue shift compared to the absorption band of AzB-DCA (shown by the green line), which indicates that the azobenzene units pack as so-called H-aggregates, with parallel orientations of the molecules.^{24,61–63} As displayed in the inset of Figure 3b, the absorbance at 320 nm increases linearly with the number of cycles, indicating a stepwise and regular film growth. Finally, it should be mentioned that all the aforementioned FTIR and UV–vis observations are in line with the schematic structure presented in Figure 1b for the $m = 0$ hybrid films.

3.3. Superlattice $m > 0$ Films. In Figure 4a, we show XRR patterns for representative $\{[(\text{Zn-O})_m + (\text{Zn-O}_2\text{-C-C}_6\text{H}_4\text{-N=N-C}_6\text{H}_4\text{-C-O}_2)]_n + (\text{Zn-O})_m\}$ thin films deposited with m ALD cycles of DEZ+H₂O to control the individual ZnO-layer thickness between monomolecular azobenzene layers deposited with a single ALD/MLD cycle. The superlattice structures can be confirmed by the presence of well-defined Kiessig fringes as well as SL peaks (demonstrated by dashed lines in Figure 4a) that are periodically repeated and correspond to the expected superlattice repeat units.⁶⁴ It is also possible to fit the XRR data for the individual layer thicknesses; we did this for the $n = 4$, $m = 240$ SL film to yield a total film thickness at 141 nm and an individual ZnO-layer thickness of 30 nm, in excellent agreement with the expected values given in Table 1.

Figure 4b shows GIXRD patterns for selected SL thin films and for a reference ZnO film. The diffraction peaks are explained well by the hexagonal wurtzite structure of ZnO and are in Figure 3b indexed accordingly. For $m < 37$, no reflections were detected, implying that the degree of crystallinity decreases when the individual ZnO-layer thickness decreases. Finally, from Figure 4c, we can see that with a decrease in m , and accordingly an increasing number (n) of organic layers (cf. Table 1), the intensity of the characteristic FTIR peaks due to the azobenzene moiety increases, as expected.

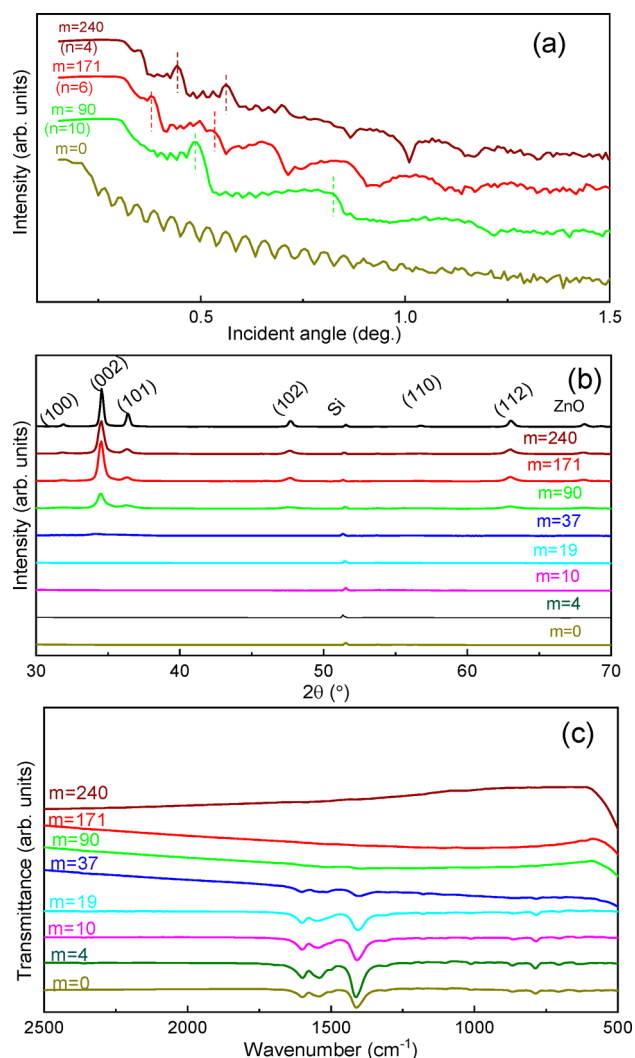


Figure 4. (a) XRR and (b) GIXRD patterns and (c) FTIR spectra for selected $\{[(\text{Zn}-\text{O})_m+(\text{Zn}-\text{O}_2-\text{C}-\text{C}_6\text{H}_4-\text{N}=\text{N}-\text{C}_6\text{H}_4-\text{C}-\text{O}_2)]_n+(\text{Zn}-\text{O})_m\}$ superlattice thin films with varying m [and n (see Table 1)].

3.4. Photoisomerization. The photoisomerization of the azobenzene moieties was investigated for our hybrid and superlattice thin films by irradiating the samples with UV light and recording the transmittance spectra at specific time intervals until a photostationary state was obtained. Figure 5 shows the changes in the UV–vis spectra during the UV light illumination for three representative as-deposited films. As the photoisomerization reaction is induced by UV light, the intensity of the $\pi-\pi^*$ band at 320 nm due to the trans isomer gradually decreases and shifts to blue while the intensity of the $n-\pi^*$ band around 400 nm that is related to the cis isomer increases. The $\pi-\pi^*$ band nearly disappears for all three samples after sufficient irradiation time, indicating an almost complete trans-to-cis photoreaction.^{17,23,65} From the insets of Figure 5, it seems that the photoisomerization reaction somewhat depends on the SL structure; this is an interesting observation to be clarified in detail in future studies.

It is well-known that the reverse cis-to-trans reaction can be realized through visible light illumination and/or thermal treatment. Because our UV–vis lamp did not allow controlled visible light illumination, we confirmed the backward cis-to-trans reaction by heating the samples at 100 °C for 24 h (see

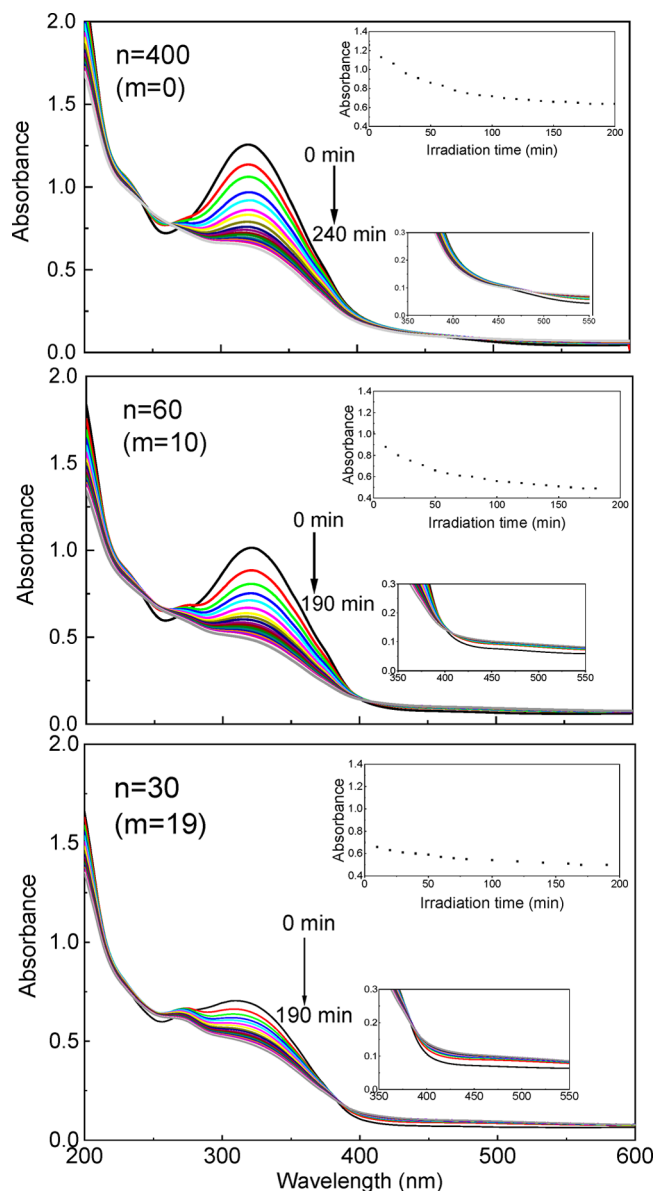


Figure 5. Changes in UV–vis spectra upon UV irradiation of as-deposited $\{[(\text{Zn}-\text{O})_m+(\text{Zn}-\text{O}_2-\text{C}-\text{C}_6\text{H}_4-\text{N}=\text{N}-\text{C}_6\text{H}_4-\text{C}-\text{O}_2)]_n+(\text{Zn}-\text{O})_m\}$ films. The top insets illustrate the kinetics of the changes.

Figure 6 for the data for the $n = 60, m = 10$ sample as an example case). One can see that the $\pi-\pi^*$ transition band that first nearly disappears upon UV irradiation increases again in intensity upon the subsequent heat treatment, indicative of the cis–trans back-isomerization of azobenzene. The complete cis-to-trans transition is hardly realized for azobenzene compounds because of the overlap of the $n-\pi^*$ transition of the trans and cis isomers.^{18,66} We confirmed the back-isomerization reaction for all of our samples, but the extent depended on the SL structure. Tentatively, we attribute this observation to the fact that the SL structure is likely to affect the optical band gap⁴³ and, thereby, the activation energy of the cis-to-trans reaction.⁶⁷ This will be systematically studied in our already initiated future work.

3.5. Morphological Changes upon Photoisomerization. Figure 7 shows XRR patterns for a hybrid $m = 0$ thin film sample before and after a 1 h irradiation. The film thickness

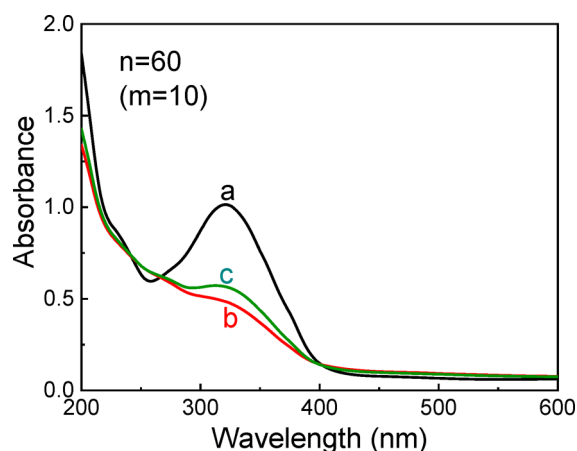


Figure 6. UV-visible absorption spectra of $\{[(\text{Zn-O})_{10}+(\text{Zn-O}_2-\text{C}-\text{C}_6\text{H}_4-\text{N}=\text{N}-\text{C}_6\text{H}_4-\text{C}-\text{O}_2)]_{60}+(\text{Zn-O})_{10}\}$: (a) the trans isomer, (b) the same sample after irradiation with UV light, and (c) the recovered trans isomer after it had been heated at 100 °C in a furnace.

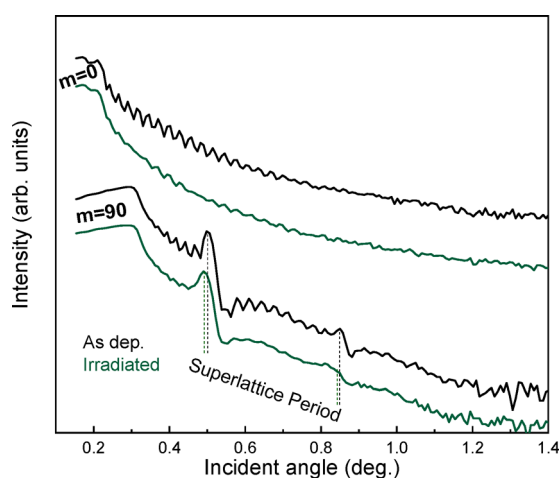


Figure 7. XRR patterns for hybrid ($m = 0$, $n = 400$) and superlattice ($m = 90$, $n = 10$) thin films. The XRR results are shown for both as-deposited films and the same films after irradiation with UV light at 365 nm for 1 h.

determined from the XRR data was found to decrease upon UV irradiation from 140 to 127 nm. Moreover, the critical angle of the XRR curves shows a clear increase with irradiation, indicating that the film density increases from 1.50 to 1.65 g/cm³. Such changes are indeed expected upon photoisomerization and the resultant contraction of the organic layers.⁴¹ Also shown in Figure 7 are similar data for a representative superlattice sample ($m = 90$); one can see that the well-defined SL structure retains after the irradiation. For the SL film, the decrease in the film thickness and the increase in density are less evident than for the hybrid film, naturally because its organic content is lower than that of the $m = 0$ case. For both the $m = 0$ and the $m = 90$ films, the interface roughness derived from the XRR fringe amplitudes seems to slightly increase (i.e., the fringe amplitude decreases) upon irradiation for 1 h.

4. CONCLUSIONS

The possibility of fusing the most exciting inorganic and organic components into a single coherent material with atomic/molecular level accuracy is highly relevant for new material research, and an elegant yet industrially feasible way to

achieve this is to exploit the ALD/MLD technique. In this work, we have demonstrated for the first time that the ALD/MLD technique can be used to incorporate fully functional photochromic organic molecules into an inorganic matrix in a highly controllable way. Moreover, as the film growth in ALD/MLD is fundamentally based on the formation of strong chemical bonds between the inorganic and organic components, strong mutual interactions between these components in the resultant thin film may be expected.

Our proof-of-concept results concerned the ZnO:azobenzene system, and the new ALD/MLD process developed in this work involved diethylzinc and azobenzene dicarboxylic acid as precursors. We were able to show that these two ALD/MLD precursors can be combined into homogeneous and stable hybrid thin films in which each azobenzene moiety, according to strong FTIR evidence, is bound to four Zn cations in such a way that both of the carboxylate groups work as a bridge between two zincs. Hybrid film growth was shown, through XRR investigation, to proceed efficiently and in an essentially ideal ALD/MLD manner at 320 °C. The high level of control furthermore allowed us to grow a series of superlattice structures in which the spacing between two consequent azobenzene layers could be accurately controlled by the number of ALD cycles applied to grow the intermittent ZnO layers from diethylzinc and water.

Finally, and most importantly, we were able to prove, through UV-vis spectroscopy measurements, that our ZnO:azobenzene superlattice structures indeed provide an amazingly suitable environment for the efficient (and reversible) photoisomerization of the azobenzene moieties upon light illumination. We believe that our ALD/MLD approach could be applied to many other inorganic/photochromic organic systems, as well, thus opening up an avenue to totally new photoswitching applications.

■ AUTHOR INFORMATION

Corresponding Author

*E-mail: maarit.karppinen@aalto.fi

ORCID

Maarit Karppinen: 0000-0003-1091-1169

Notes

The authors declare no competing financial interest.

■ ACKNOWLEDGMENTS

This work was supported by the European Research Council under the European Union's Seventh Framework Programme (FP/2007-2013)/ERC Advanced Grant Agreement (339478) and the Academy of Finland (296299).

■ REFERENCES

- (1) Gorostiza, P.; Isacoff, E. Y. Optical Switches for Remote and Noninvasive Control of Cell Signaling. *Science* **2008**, *322*, 395–399.
- (2) Que, W. X.; Yao, X.; Liu, W. G. Azobenzene-Containing Small Molecules Organic-Inorganic Hybrid Sol-Gel Materials for Photonic Applications. *Appl. Phys. B: Lasers Opt.* **2008**, *91*, 539–543.
- (3) Hu, D.; Lin, J.; Jin, S.; Hu, Y.; Wang, W.; Wang, R.; Yang, B. Synthesis, Structure and Optical Data Storage Properties of Silver Nanoparticles Modified with Azobenzene Thiols. *Mater. Chem. Phys.* **2016**, *170*, 108–112.
- (4) Spiridon, M. C.; Iliopoulos, K.; Jerca, F. A.; Jerca, V. V.; Vuluga, D. M.; Vasilescu, D. S.; Gindre, D.; Sahrroui, B. Novel Pendant Azobenzene/Polymer Systems for Second Harmonic Generation and Optical Data Storage. *Dyes Pigm.* **2015**, *114*, 24–32.

- (5) Tarn, D.; Ferris, D. P.; Barnes, J. C.; Ambrogio, M. W.; Stoddart, J. F.; Zink, J. I. A Reversible Light-Operated Nanovalve on Mesoporous Silica Nanoparticles. *Nanoscale* **2014**, *6*, 3335–3343.
- (6) Joshi, G. K.; Blodgett, K. N.; Muhoberac, B. B.; Johnson, M. A.; Smith, K. A.; Sardar, R. Ultrasensitive Photoreversible Molecular Sensors of Azobenzene-Functionalized Plasmonic Nanoantennas. *Nano Lett.* **2014**, *14*, 532–540.
- (7) Pearson, S.; Vitucci, D.; Khine, Y. Y.; Dag, A.; Lu, H.; Save, M.; Billon, L.; Stenzel, M. H. Light-Responsive Azobenzene-Based Glycopolymer Micelles for Targeted Drug Delivery to Melanoma Cells. *Eur. Polym. J.* **2015**, *69*, 616–627.
- (8) Deka, S. R.; Yadav, S.; Mahato, M.; Sharma, A. K. Azobenzene-Aminoglycoside: Self-Assembled Smart Amphiphilic Nanostructures for Drug Delivery. *Colloids Surf., B* **2015**, *135*, 150–157.
- (9) Gu, W.-X.; Li, Q.-L.; Lu, H.; Fang, L.; Chen, Q.; Yang, Y.-W.; Gao, H. Construction of Stable Polymeric Vesicles Based on Azobenzene and Beta-Cyclodextrin Grafted Poly(Glycerol Methacrylate)s for Potential Applications in Colon-Specific Drug Delivery. *Chem. Commun.* **2015**, *51*, 4715–4718.
- (10) Que, W.; Hu, X.; Xia, X. L.; Zhao, L. Photo-Responsive Properties of Azobenzene Small Molecules in Sol-Gel Hybrid TiO₂/Ormosil Organic-Inorganic Matrices. *Opt. Express* **2007**, *15*, 480–485.
- (11) Heinz, H.; Vaia, R. A.; Koerner, H.; Farmer, B. L. Photoisomerization of Azobenzene Grafted to Layered Silicates: Simulation and Experimental Challenges. *Chem. Mater.* **2008**, *20*, 6444–6456.
- (12) Rad, F. A.; Rezvani, Z.; Khodam, F. Molecular Design Confirmation for Proposition of Improved Photophysical Properties in a Dye-Intercalated Layered Double Hydroxides. *RSC Adv.* **2016**, *6*, 11193–11203.
- (13) Henningsen, N.; Rurali, R.; Franke, K. J.; Fernández-Torrente, I.; Pascual, J. I. Trans to Cis Isomerization of an Azobenzene Derivative on a Cu(100) Surface. *Appl. Phys. A: Mater. Sci. Process.* **2008**, *93*, 241–246.
- (14) Kume, S.; Kurihara, M.; Nishihara, H. Reversible Trans–Cis Photoisomerization of Azobenzene-Attached Bipyridine Ligands Coordinated to Cobalt Using a Single UV Light Source and the Co(III)/Co(II) Redox Change. *Chem. Commun.* **2001**, *6*, 1656–1657.
- (15) Shembekar, V. R.; Contractor, A. Q.; Major, S. S.; Talwar, S. S. Photoisomerization of Amphiphilic Azobenzene Derivatives in Langmuir Blodgett Films Prepared as Polyion Complexes, Using Ionic Polymers. *Thin Solid Films* **2006**, *510*, 297–304.
- (16) Conti, I.; Garavelli, M.; Orlandi, G. The Different Photoisomerization Efficiency of Azobenzene in the Lowest $n\pi^*$ and $\pi\pi^*$ Singlets: The Role of a Phantom State. *J. Am. Chem. Soc.* **2008**, *130*, 5216–5230.
- (17) Abellán, G.; Coronado, E.; Martí-Gastaldo, C.; Ribera, A.; Jordá, J. L.; García, H. Photo-Switching in a Hybrid Material Made of Magnetic Layered Double Hydroxides Intercalated with Azobenzene Molecules. *Adv. Mater.* **2014**, *26*, 4156–4162.
- (18) Han, J.; Yan, D.; Shi, W.; Ma, J.; Yan, H.; Wei, M.; Evans, D. G.; Duan, X. Layer-by-Layer Ultrathin Films of Azobenzene-Containing Polymer/Layered Double Hydroxides with Reversible Photoresponsive Behavior. *J. Phys. Chem. B* **2010**, *114*, 5678–5685.
- (19) Xia, S. J.; Liu, F. X.; Ni, Z. M.; Shi, W.; Xue, J. L.; Qian, P. P. Ti-Based Layered Double Hydroxides: Efficient Photocatalysts for Azo Dyes Degradation under Visible Light. *Appl. Catal., B* **2014**, *144*, 570–579.
- (20) Iwicki, J.; Ludwig, E.; Källäne, M.; Buck, J.; Köhler, F.; Herges, R.; Kipp, L.; Rossnagel, K. Photoswitching of Azobenzene Multilayers on a Layered Semiconductor. *Appl. Phys. Lett.* **2010**, *97* (1–3), 063112.
- (21) Abellán, G.; García, H.; Gómez-García, C. J.; Ribera, A. Photochemical Behavior in Azobenzene Having Acidic Groups. Preparation of Magnetic Photoresponsive Gels. *J. Photochem. Photobiol., A* **2011**, *217*, 157–163.
- (22) Sun, M.; Que, W.; Hu, X. Preparation and Trans-Cis Isomerization of Azobenzene-Containing TiO₂/Ormosils Hybrid Films Derived at a Low Temperature Sol-Gel Process for Photonic Applications. *J. Sol-Gel Sci. Technol.* **2009**, *50*, 415–420.
- (23) Shah, S. M.; Martini, C.; Ackermann, J.; Fages, F. Photo-switching in Azobenzene Self-Assembled Monolayers Capped on Zinc Oxide: Nanodots vs Nanorods. *J. Colloid Interface Sci.* **2012**, *367*, 109–114.
- (24) Wu, A.; Talham, D. R. Photoisomerization of Azobenzene Chromophores in Organic/Inorganic Zirconium Phosphonate Thin Films Prepared Using a Combined Langmuir-Blodgett and Self-Assembled Monolayer Deposition. *Langmuir* **2000**, *16*, 7449–7456.
- (25) Pardo, R.; Zayat, M.; Levy, D. Photochromic Organic–inorganic Hybrid Materials. *Chem. Soc. Rev.* **2011**, *40*, 672–678.
- (26) Nilsen, O.; Klepper, K. B.; Nielsen, H.; Fjellvåg, H. Deposition of Organic–Inorganic Hybrid Materials by Atomic Layer Deposition. *ECS Trans.* **2008**, *16*, 3–14.
- (27) George, S. M. Atomic Layer Deposition: An Overview. *Chem. Rev.* **2010**, *110*, 111–131.
- (28) Knez, M.; Nielsch, K.; Niinistö, L. Synthesis and Surface Engineering of Complex Nanostructures by Atomic Layer Deposition. *Adv. Mater.* **2007**, *19*, 3425–3438.
- (29) Miikkulainen, V.; Leskelä, M.; Ritala, M.; Puurunen, R. L. Crystallinity of Inorganic Films Grown by Atomic Layer Deposition: Overview and General Trends. *J. Appl. Phys.* **2013**, *113*, 021301.
- (30) Yoshimura, T.; Tatsuura, S.; Sotoyama, W. Polymer Films Formed with Monolayer Growth Steps by Molecular Layer Deposition. *Appl. Phys. Lett.* **1991**, *59*, 482–484.
- (31) Kubono, A.; Yuasa, N.; Shao, H.-L.; Umemoto, S.; Okui, N. In-Situ Study on Alternating Vapor Deposition Polymerization of Alkyl Polyamide with Normal Molecular Orientation. *Thin Solid Films* **1996**, *289*, 107–111.
- (32) Sundberg, P.; Karppinen, M. Organic-Inorganic Thin Films from TiCl₄ and 4-Aminophenol Precursors: A Model Case of ALD/MLD Hybrid-Material Growth. *Eur. J. Inorg. Chem.* **2014**, *2014*, 968–974.
- (33) Johnson, R. W.; Hultqvist, A.; Bent, S. F. A Brief Review of Atomic Layer Deposition: From Fundamentals to Applications. *Mater. Mater. Today* **2014**, *17*, 236–246.
- (34) Krah, F.; Giri, A.; Tomko, J. A.; Tynell, T.; Hopkins, P. E.; Karppinen, M. Thermal Conductivity Reduction at Inorganic–Organic Interfaces: From Regular Superlattices to Irregular Gradient Layer Sequences. *Adv. Mater. Interfaces* **2018**, *5* (1–7), 1701692.
- (35) Tynell, T.; Terasaki, I.; Yamauchi, H.; Karppinen, M. Thermoelectric Characteristics of (Zn,Al)O/Hydroquinone Superlattices. *J. Mater. Chem. A* **2013**, *1*, 13619–13624.
- (36) Tynell, T.; Karppinen, M. ZnO: Hydroquinone Superlattice Structures Fabricated by Atomic/Molecular Layer Deposition. *Thin Solid Films* **2014**, *551*, 23–26.
- (37) Vähä-Nissi, M.; Sundberg, P.; Kauppi, E.; Hirvikorpi, T.; Sievänen, J.; Sood, A.; Karppinen, M.; Harlin, A. Barrier Properties of Al₂O₃ and Alucone Coatings and Nanolaminates on Flexible Biopolymer Films. *Thin Solid Films* **2012**, *520*, 6780–6785.
- (38) Xiao, W.; Hui, D. Y.; Zheng, C.; Yu, D.; Qiang, Y. Y.; Ping, C.; Xiang, C. L.; Yi, Z. A Flexible Transparent Gas Barrier Film Employing the Method of Mixing ALD/MLD-Grown Al₂O₃ and Alucone Layers. *Nanoscale Res. Lett.* **2015**, *10*, 1–7.
- (39) Yoon, K. H.; Kim, H. S.; Han, K. S.; Kim, S. H.; Lee, Y. E. K.; Shrestha, N. K.; Song, S. Y.; Sung, M. M. Extremely High Barrier Performance of Organic-Inorganic Nanolaminated Thin Films for Organic Light-Emitting Diodes. *ACS Appl. Mater. Interfaces* **2017**, *9*, 5399–5408.
- (40) Tynell, T.; Giri, A.; Gaskins, J.; Hopkins, P. E.; Mele, P.; Miyazaki, K.; Karppinen, M. Efficiently Suppressed Thermal Conductivity in ZnO Thin Films via Periodic Introduction of Organic Layers. *J. Mater. Chem. A* **2014**, *2*, 12150–12152.
- (41) Niemelä, J.-P.; Giri, A.; Hopkins, P. E.; Karppinen, M. Ultra-Low Thermal Conductivity in TiO₂:C Superlattices. *J. Mater. Chem. A* **2015**, *3*, 11527–11532.
- (42) Karttunen, A. J.; Tynell, T.; Karppinen, M. Layer-by-Layer Design of Nanostructured Thermoelectrics: First-Principles Study of

ZnO: Organic Superlattices Fabricated by ALD/MLD. *Nano Energy* **2016**, *22*, 338–348.

(43) Niemelä, J.-P.; Karppinen, M. Tunable Optical Properties of Hybrid Inorganic–Organic [(TiO₂)_m(Ti–O–C₆H₄–O)_k]_n Superlattice Thin Films. *Dalt. Trans.* **2015**, *44*, 591–597.

(44) Meng, X. An Overview of Molecular Layer Deposition for Organic and Organic–Inorganic Hybrid Materials: Mechanisms, Growth Characteristics, and Promising Applications. *J. Mater. Chem. A* **2017**, *5*, 18326–18378.

(45) Tynell, T.; Karppinen, M. Atomic Layer Deposition of ZnO: A Review. *Semicond. Sci. Technol.* **2014**, *29* (1–15), 043001.

(46) Janotti, A.; Van De Walle, C. G. Fundamentals of Zinc Oxide as a Semiconductor. *Rep. Prog. Phys.* **2009**, *72* (1–29), 126501.

(47) Klingshirn, C. ZnO: From Basics towards Applications. *Phys. Status Solidi B* **2007**, *244*, 3027–3073.

(48) Yousfi, E. B.; Fouache, J.; Lincot, D. Study of Atomic Layer Epitaxy of Zinc Oxide by In-Situ Quartz Crystal Microgravimetry. *Appl. Surf. Sci.* **2000**, *153*, 223–234.

(49) Elam, J. W.; Sechrist, Z. A.; George, S. M. ZnO/Al₂O₃ Nanolaminates Fabricated by Atomic Layer Deposition: Growth and Surface Roughness Measurements. *Thin Solid Films* **2002**, *414*, 43–55.

(50) Yoon, B.; O’Patches, J. L.; Seghete, D.; Cavanagh, A. S.; George, S. M. Molecular Layer Deposition of Hybrid Organic–Inorganic Polymer Films Using Diethylzinc and Ethylene Glycol. *Chem. Vap. Deposition* **2009**, *15*, 112–121.

(51) Peng, Q.; Gong, B.; VanGundy, R. M.; Parsons, G. N. Zinc Oxide - Organic Hybrid Polymer Thin Films Formed by Molecular Layer Deposition. *Chem. Mater.* **2009**, *21*, 820–830.

(52) Sood, A.; Sundberg, P.; Karppinen, M. ALD/MLD of Novel Layer-Engineered Zn-Based Inorganic–Organic Hybrid Thin Films Using Heterobifunctional 4-Aminophenol as an Organic Precursor. *Dalt. Trans.* **2013**, *42*, 3869–3875.

(53) Yoon, B.; Lee, B. H.; George, S. M. Highly Conductive and Transparent Hybrid Organic–Inorganic Zinc Oxide Thin Films Using Atomic and Molecular Layer Deposition. *J. Phys. Chem. C* **2012**, *116*, 24784–24791.

(54) Choudhury, D.; Sarkar, S. K. The ALD-MLD Growth of a ZnO-Zinc Oxide Heterostructure. *Chem. Vap. Deposition* **2014**, *20*, 130–137.

(55) Yang, J. L.; An, S. J.; Park, W. I.; Yi, G.-C.; Choi, W. Photocatalysis Using ZnO Thin Films and Nanoneedles Grown by Metal–Organic Chemical Vapor Deposition. *Adv. Mater.* **2004**, *16*, 1661–1664.

(56) Wang, C.; Wang, X.; Xu, B. Q.; Zhao, J.; Mai, B.; Peng, P.; Sheng, G.; Fu, J. Enhanced Photocatalytic Performance of Nanosized Coupled ZnO/SnO₂ Photocatalysts for Methyl Orange Degradation. *J. Photochem. Photobiol., A* **2004**, *168*, 47–52.

(57) Bae, J.; Han, J. B.; Zhang, X.-M.; Wei, M.; Duan, X.; Zhang, Y.; Wang, Z. L. ZnO Nanotubes Grown at Low Temperature Using Ga as Catalysts and Their Enhanced Photocatalytic Activities. *J. Phys. Chem. C* **2009**, *113*, 10379–10383.

(58) Pung, S.-Y.; Choy, K.-L.; Hou, X.; Shan, C. Preferential Growth of ZnO Thin Films by the Atomic Layer Deposition Technique. *Nanotechnology* **2008**, *19*, 435609.

(59) Klepper, K. B.; Nilsen, O.; Levy, T.; Fjellvåg, H. Atomic Layer Deposition of Organic–Inorganic Hybrid Materials Based on Unsaturated Linear Carboxylic Acids. *Eur. J. Inorg. Chem.* **2011**, *2011*, 5305–5312.

(60) Penttinen, J.; Nisula, M.; Karppinen, M. Atomic/Molecular Layer Deposition of s-Block Metal Carboxylate Coordination Network Thin Films. *Chem. - Eur. J.* **2017**, *23*, 18225–18231.

(61) Haruta, O.; Matsuo, Y.; Ijiri, K. Photo-Induced Fluorescence Emission Enhancement of Azobenzene Thin Films. *Colloids Surf., A* **2008**, *313–314*, 595–599.

(62) Petruska, M. A.; Talham, D. R. Organic/Inorganic Langmuir–Blodgett Films Based on Metal Phosphonates. 3. An Azobenzene-Derivatized Phosphonic Acid Forms Continuous Lattice Layers with Divalent, Trivalent, and Tetravalent Metal Ions 1. *Chem. Mater.* **1998**, *10*, 3672–3682.

(63) Kawai, T.; Umemura, J.; Takenaka, T. UV Absorption Spectra of Azobenzene-Containing Long-Chain Fatty Acids and Their Barium Salts in Spread Monolayers and Langmuir–Blodgett Films. *Langmuir* **1989**, *5*, 1378–1383.

(64) Chopdekar, R. V.; Malik, V. K.; Kane, A. M.; Mehta, A.; Arenholz, E.; Takamura, Y. Engineered Superlattices with Crossover from Decoupled to Synthetic Ferromagnetic Behavior. *J. Phys.: Condens. Matter* **2018**, *30* (1–8), 015805.

(65) Nabetani, Y.; Takamura, H.; Hayasaka, Y.; Sasamoto, S.; Tanamura, Y.; Shimada, T.; Masui, D.; Takagi, S.; Tachibana, H.; Tong, Z.; et al. An Artificial Muscle Model Unit Based on Inorganic Nanosheet Sliding by Photochemical Reaction. *Nanoscale* **2013**, *5*, 3182–3193.

(66) Wu, Z.; Xue, R.; Xie, M.; Wang, X.; Liu, Z.; Drechsler, M.; Huang, J.; Yan, Y. Self-Assembly-Triggered Cis-to-Trans Conversion of Azobenzene Compounds. *J. Phys. Chem. Lett.* **2018**, *9*, 163–169.

(67) Ramakrishnan, V.; Yamamoto, D.; Sasamoto, S.; Shimada, T.; Nabetani, Y.; Tachibana, H.; Inoue, H. Remarkable Enhancement of the Photoreactivity of a Polyfluoroalkyl Azobenzene Derivative in an Organic–Inorganic Nano-Layered Microenvironment. *Phys. Chem. Chem. Phys.* **2014**, *16*, 23663–23670.